Chandra Observations of High-energy X-Ray Sources Discovered by *INTEGRAL*

John A. Tomsick[1] , Arash Bodaghee[2] , Sylvain Chaty[3,4], Maïca Clavel[5] , Francesca M. Fornasini[6] , Jeremy Hare[1,7,10] ,
Roman Krivonos[8] , Farid Rahoui[9] , and Jerome Rodriguez[3]

[1] Space Sciences Laboratory, 7 Gauss Way, University of California, Berkeley, CA 94720-7450, USA
[2] Georgia College & State University, CBX 82, Milledgeville, GA 31061, USA
[3] AIM, CEA, CNRS, Université Paris-Saclay, Université Paris Diderot, Sorbonne Paris Cité, F-91191 Gif-sur-Yvette, France
[4] APC, Université Paris Diderot, CNRS/IN2P3, CEA/IRFU, Observatoire de Paris, Sorbonne Paris Cité, Paris 75205, France
[5] Univ. Grenoble Alpes, CNRS, IPAG, F-38000 Grenoble, France
[6] Harvard-Smithsonian Center for Astrophysics, 60 Garden Street, Cambridge, MA 02138, USA
[7] NASA Goddard Space Flight Center, Greenbelt, MD 20771, USA
[8] Space Research Institute, Russian Academy of Sciences, Profsoyuznaya 84/32, 117997 Moscow, Russia
[9] Independent, France

Abstract

The *International Gamma-Ray Astrophysics Laboratory* (*INTEGRAL*) satellite has detected in excess of 1000 sources in the ~20–100 keV band during its surveys of the sky over the past 17 years. We obtained 5 ks observations of 15 unclassified *INTEGRAL* Gamma-Ray (IGR) sources with the *Chandra X-ray Observatory* in order to localize them, to identify optical/IR counterparts, to measure their soft X-ray spectra, and to classify them. For 10 of the IGR sources, we detect *Chandra* sources that are likely (or in some cases certain) to be the counterparts. IGR J18007–4146 and IGR J15038–6021 both have *Gaia* parallax distances, placing them at $2.5^{+0.5}_{-0.4}$ and $1.1^{+1.5}_{-0.4}$ kpc, respectively. We tentatively classify both of them as intermediate polar-type cataclysmic variables. Also, IGR J17508–3219 is likely to be a Galactic source, but it is unclear if it is a Dwarf Nova or another type of transient. For IGR J17118–3155, we provide a *Chandra* localization, but it is unclear if the source is Galactic or extragalactic. Based on either near-IR/IR colors or the presence of extended near-IR emission, we classify four sources as active galactic nuclei (AGNs; IGR J16181–5407, IGR J16246–4556, IGR J17096–2527, and IGR J19294+1327), and IGR J20310+3835 and IGR J15541–5613 are AGN candidates. In addition, we identified an AGN in the *INTEGRAL* error circle of IGR J16120–3543 that is a possible counterpart.

Unified Astronomy Thesaurus concepts: X-ray sources (1822); Cataclysmic variable stars (203); High mass X-ray binary stars (733); Active galactic nuclei (16); Galaxy stellar content (621)

1. Introduction

Since 2002, the *International Gamma-Ray Astrophysics Laboratory* (*INTEGRAL*) satellite has been carrying out observations with its large field of view coded aperture mask instruments (Winkler et al. 2003). In particular, as the exposure time in the ~20–100 keV band across the sky and especially in the Galactic plane has increased, more new or previously poorly studied "*INTEGRAL* Gamma-Ray" (IGR) sources have been found. *INTEGRAL* has now detected in excess of 1000 sources (Bird et al. 2016; Krivonos et al. 2017) with the majority being new sources.

The hard X-ray bandpass of *INTEGRAL* provides a way to select sources where extreme physics is occurring. The high-energy emission can be produced by accretion onto a compact object (magnetic white dwarf, neutron star, or black hole) or when particle acceleration leads to nonthermal emission. The Bird et al. (2016) *INTEGRAL* source catalog includes 939 sources. Over the whole sky, active galactic nuclei (AGNs) dominate and account for 369 of the sources. The Galactic population is dominated by 129 low mass X-ray binaries, 116 high mass X-ray binaries (HMXBs), and 56 cataclysmic variables (CVs). Pulsar wind nebulae (PWNe), supernova remnants, and galaxy clusters are also among the IGR sources. Thus, *INTEGRAL* is providing a much more complete picture of the populations of hard X-ray sources, and making discoveries about Galactic sources, including two new classes of

HMXBs: obscured HMXBs (Matt & Guainazzi 2003; Walter et al. 2006) and Supergiant Fast X-ray Transients (Negueruela et al. 2006; Sguera et al. 2006; Romano et al. 2014); larger numbers of hard X-ray emitting intermediate polars (IPs; Bonnet-Bidaud et al. 2007; Landi et al. 2009; Tomsick et al. 2016b); and highly energetic PWNe (Tomsick et al. 2012b; Pavan et al. 2014).

While *INTEGRAL* excels at detecting sources in the 20–100 keV band, it only localizes the sources to 1′–5′, which is not adequate for finding optical/IR counterparts. Thus, in most cases, sources are not classified until higher angular resolution X-ray observations are obtained, providing an image to identify extended sources or to improve the source localization, allowing for multiwavelength counterparts to be found. Large X-ray follow-up programs include the use of the *Neil Gehrels Swift Observatory* X-ray Telescope (*Swift*/XRT; Landi et al. 2017, and references therein) and the *Chandra X-ray Observatory* (e.g., Tomsick et al. 2006, 2008, 2016a). The X-ray localizations enable optical and near-IR spectroscopy (e.g., Chaty et al. 2008; Coleiro et al. 2013; Masetti et al. 2013; Fortin et al. 2018), at which point confident source classifications are nearly always obtained.

1.1. Target Selection

When the Bird et al. (2016) catalog was released, there were 219 unidentified sources in the catalog, and we selected sources to observe with *Chandra* based on the following criteria:

---

[10] NASA Postdoctoral Program Fellow.

Table 1
Source Information from the 2016 *INTEGRAL* Catalog

IGR Name	l[a] (deg)	b[b] (deg)	R.A.[c] (deg)	Decl.[c] (deg)	Uncertainty[d] (arcmin)	Flux[e] (20–40 keV)	Flux[e] (40–100 keV)	Variability[f]	Significance[g]
J20310+3835	77.77	−0.49	307.755	+38.576	4.54	0.6 ± 0.1	<0.3	⋯	5.5
J15038−6021	318.60	−1.57	225.941	−60.357	3.95	0.5 ± 0.1	0.4 ± 0.2	⋯	6.4
J03599+5043	150.58	−1.74	59.973	+50.728	4.01	0.7 ± 0.2	1.2 ± 0.3	Y	6.3
J15541−5613	326.38	−1.90	238.527	−56.216	4.32	<0.2	0.8 ± 0.2	Y	5.8
J19294+1327	49.22	−2.12	292.374	+13.451	3.43	0.5 ± 0.1	0.5 ± 0.1	⋯	7.5
J16246−4556	336.83	+2.46	246.091	−45.923	4.61	0.4 ± 0.1	<0.3	Y	5.4
J16181−5407	330.35	−2.62	244.533	−54.103	4.61	0.5 ± 0.1	0.4 ± 0.1	⋯	5.4
J17508−3219	357.68	−2.72	267.721	−32.330	2.31	0.6 ± 0.1	0.9 ± 0.1	⋯	11.6
J17118−3155	353.48	+4.41	257.959	−31.927	2.84	0.3 ± 0.1	<0.2	Y	9.2
J20413+3210	73.96	−6.02	310.384	+32.219	3.42	<0.3	<0.4	Y	7.5
J07202+0009	216.12	+6.47	110.063	+0.127	4.25	<0.4	<0.7	Y	5.9
J17096−2527	358.47	+8.56	257.432	−25.470	2.73	0.8 ± 0.1	0.8 ± 0.1	⋯	9.6
J18007−4146	350.38	−9.12	270.202	−41.802	3.19	0.9 ± 0.1	0.5 ± 0.2	⋯	8.1
J16482−2959	351.94	+9.52	252.145	−30.019	4.25	0.3 ± 0.1	0.6 ± 0.2	Y	5.9
J16120−3543	342.36	+11.35	242.974	−35.754	4.69	0.4 ± 0.2	0.6 ± 0.3	Y	5.3

Notes.
[a] Galactic longitude converted from *INTEGRAL* position.
[b] Galactic latitude converted from *INTEGRAL* position.
[c] Source position measured by *INTEGRAL* and reported in Bird et al. (2016).
[d] 90% confidence *INTEGRAL* error radius.
[e] The flux measured by *INTEGRAL* in units of mCrab.
[f] As described in Bird et al. (2016), "Y" indicates that the source's detection significance in the *INTEGRAL* data is variable at a level of between 10% and 400%.
[g] The significance of the *INTEGRAL* detection in terms of signal-to-noise.

1. the selected sources have IGR names, indicating discovery in the hard X-rays by *INTEGRAL*;
2. the nature is completely unknown for the selected sources (i.e., the type is listed as "?");
3. the sources are "new" in that they did not appear in the Bird et al. (2010) catalog, implying that there has been little opportunity for follow-up observations; and
4. they are within 15° of the Galactic plane, increasing the chances that they are Galactic (we note that the highest Galactic latitude in our final list is $b = 11°35$).

After applying these four criteria, 56 sources remained, but we reduced the list further based on available information about performed or planned observations with *Chandra*, the *X-ray Multi-Mirror Mission* (*XMM-Newton*), and *Swift*. For example, when we selected targets, 20 of the 56 sources had planned *Swift* observations, and these were removed from our list (although we kept some sources that already had *Swift* observations after confirming that the *Swift* localization did not identify a unique optical or near-IR counterpart). We also found that some of the sources show evidence for being variable or strongly variable in the hard X-rays based on the analysis of Bird et al. (2016). Strong variability (changes in *INTEGRAL* detection significance over time by >400%) could indicate that the source is truly transient, which means that it could be too faint to be detected in a short *Chandra* observation, and so none of the sources in our final list are in the strongly variable category. However, most Galactic sources (and certainly X-ray binaries) are variable, so we kept the sources in the variable category (changes in *INTEGRAL* detection significance over time by between 10% and 400%), and these are indicated in Table 1.

After the above considerations, the list of 15 IGR sources in Table 1 remained. They were observed with *Chandra*, and we describe the observations in Section 2. In Section 3, we describe the analysis of the data and present the results. The primary goal is to obtain X-ray positions of the IGR sources with subarcsecond accuracy, but this also includes assessing which is the most likely *Chandra* counterpart for each IGR source. For this, we follow methods that are similar to those we have developed in earlier works (Tomsick et al. 2009, 2012a). We discuss the results in Section 4 and summarize our conclusions in Section 5.

2. *Chandra* Observations

The list of IGR targets and information about the *Chandra* observations is provided in Table 2. For all 15 observations, the target was observed with the ACIS-I instrument (Garmire et al. 2003), which has a bandpass of 0.3–10 keV. IGR sources are typically relatively bright, with X-ray fluxes of $\sim 10^{-12}$ erg cm^{-2} s^{-1}. At these flux levels, exposure times of ~ 5 ks are sufficient to detect tens or hundreds of counts, depending on spectral shape and variability. Although some highly absorbed or highly variable IGR sources could have significantly lower X-ray flux levels, longer exposure times would not necessarily lead to the identification of the *Chandra* counterpart. With the 90% confidence *INTEGRAL* error circles having radii between $2'31$ and $4'69$, we would expect the sky density of field sources to make it difficult to select the true counterpart if it had a significantly lower X-ray flux level than expected.

Table 2 also provides the pointing positions used for each IGR source. In 11 cases, we simply used the *INTEGRAL* position reported in the Bird et al. (2016) catalog. However, for four sources (IGR J19294+1327, IGR J16181−5407, IGR J20310 +3835, and IGR J18007−4146), *Swift*/XRT observations identified a possible counterpart, and we used the XRT position for the *Chandra* pointing. However, in each case, the full *INTEGRAL* error circle was included in the ACIS-I field of

Table 2
Chandra Observations

IGR Name	ObsID	Start Time (UT)	Exposure Time (s)	R.A. (deg)	Decl. (deg)	Reference
J20310+3835	18969	2017 Feb 26, 19.2 hr	4880	307.73052	+38.56095	our analysis[a]
J15038−6021	18970	2017 Apr 26, 13.5 hr	4899	225.941	−60.357	Bird et al. (2016)
J03599+5043	18971	2017 Mar 20, 1.8 hr	5056	59.973	+50.728	Bird et al. (2016)
J15541−5613	18972	2017 May 22, 5.3 hr	4995	238.527	−56.216	Bird et al. (2016)
J19294+1327	18973	2017 Feb 24, 5.9 hr	4880	292.37417	+13.45151	Pavan et al. (2011)
J16246−4556	18974	2017 May 3, 12.6 hr	4886	246.091	−45.923	Bird et al. (2016)
J16181−5407	18975	2017 May 20, 14.1 hr	5019	244.53342	−54.10272	Landi et al. (2012)
J17508−3219	18976	2017 May 8, 22.6 hr	5013	267.721	−32.330	Bird et al. (2016)
J17118−3155	18977	2017 Jan 27, 16.8 hr	4883	257.959	−31.927	Bird et al. (2016)
J20413+3210	18978	2017 Feb 24, 7.8 hr	4730	310.384	+32.219	Bird et al. (2016)
J07202+0009	18979	2017 Sep 9, 18.1 hr	4899	110.063	+0.127	Bird et al. (2016)
J17096−2527	18980	2017 Jan 25, 11.0 hr	4845	257.432	−25.470	Bird et al. (2016)
J18007−4146	18981	2017 Aug 22, 5.2 hr	4994	270.17792	−41.78028	our analysis[a]
J16482−2959	18982	2017 Jun 20, 15.6 hr	4979	252.145	−30.019	Bird et al. (2016)
J16120−3543	18983	2017 Mar 31, 16.8 hr	4880	242.974	−35.754	Bird et al. (2016)

Note.
[a] We determined this position via analysis of *Swift*/XRT data. The XRT position is now published in Landi et al. (2017).

view, and in searching for the IGR source, we considered our search region to be the *INTEGRAL* error circle.

3. Analysis and Results

3.1. Chandra Source Detection, Localization, and Photometry

We reduced the data using the *Chandra* Interactive Analysis of Observations (CIAO; Fruscione et al. 2006) version 4.11 software along with the Calibration Database version 4.8.4.1. We used chandra_repro to reprocess the data, which results in an event list along with several other files with information about the spacecraft aspect, bad detector pixels, etc. After reprocessing, the steps in our analysis are to search for sources on the four ACIS-I detector chips, cross-correlate with the *Gaia* Data Release 2 (DR2) optical source catalog (Prusti et al. 2016; Gaia Collaboration et al. 2018) to register the images and reduce the contribution of the systematic pointing uncertainty to the source localization uncertainties, and perform aperture photometry to determine the number of counts for each detected source. We generally follow the instructions in the CIAO science threads.[11]

For each of the 15 observations, we used fluximage to produce an exposure-corrected image in the 0.3–10 keV energy band, and applied the wavdetect source detection algorithm to this image with wavelet scales of 1, 2, 4, 6, 8, 12, 16, 24, and 32 and the detection threshold set at a level to produce a list of sources for which only one spurious source is expected. Table 3 shows that between 6 and 28 *Chandra* sources were detected per ObsID. We used the imaging program SAOImage (ds9) to search the *Gaia* DR2 catalog for optical sources in the ACIS-I field and cross-correlated the *Chandra* and *Gaia* source lists using CIAO's wcs_match. For 11 of the ObsIDs, between 3 and 7 matches were found, allowing for a position shift to be calculated to register the *Chandra* image to the *Gaia* reference frame. The shifts are listed in Table 3 along with the average residuals between the *Chandra* and *Gaia* positions, which are between 0″32 and 0″63. We take these values to be the systematic pointing uncertainty. The four remaining

ObsIDs have zero or one match, and we do not perform any position shifts for these. Thus, the systematic pointing uncertainty in these four cases is 0″8 (90% confidence).[12]

We carried out the *Chandra* aperture photometry to determine the number of counts for all of the detected sources. We made a point-spread function (PSF) map using mkpsfmap for an energy of 2.3 keV (the typical average photon energy for the full 0.3–10 keV *Chandra* bandpass), and determined the 95% encircled energy radius for each source. After defining large (typically ~15 arcmin^2) source-free background regions for each observation, we used dmextract to extract background-subtracted counts in the 0.3–2 keV, 2–10 keV, and 0.3–10 keV energy bands. Based on our previous work (e.g., Tomsick et al. 2012a), for each source we calculated the probability that the source would be detected in a search area with a radius of θ_{search}. In cases where the source is within the 90% confidence *INTEGRAL* error radius ($\theta_{INTEGRAL}$), $\theta_{search} = \theta_{INTEGRAL}$. If the source is outside the *INTEGRAL* error radius then θ_{search} is equal to the angular distance from the best estimate of the *INTEGRAL* position.

The predicted surface density of sources is the other factor that is important for determining the spurious source probability. In Tomsick et al. (2012a), we used

$$N(>F_{2-10\,keV}) = 9.2(F_{2-10\,keV}/10^{-13})^{-0.79}\,deg^{-2}, \quad (1)$$

which is based on the $\log N$-$\log S$ curve from the *Advanced Satellite for Cosmology and Astrophysics* (Sugizaki et al. 2001). However, this work only included the Galactic sources, so we also consider a more recent determination of the $\log N$-$\log S$ in the Norma Region of the Galactic Plane

$$N(>F_{2-10\,keV}) = 36(F_{2-10\,keV}/10^{-13})^{-1.24}\,deg^{-2}, \quad (2)$$

which also includes AGNs (Fornasini et al. 2014). In addition, the Norma Region is centered on the Galactic plane, covering $-0°.4 < b < 0°.4$, likely representing an upper bound on the source density. While we use these exact equations in Section 3.2 to determine the absolute spurious source

Table 3
Source Detection and Shifts Based on *Gaia* DR2 Matches

IGR Name	ObsID	$N_{Chandra}$[a]	$N_{\rm matches}$[b]	$x_{\rm shift}$[c]	$y_{\rm shift}$[c]	Residual[d]
J20310+3835	18969	11	5	−0.46	0.75	0.34
J15038–6021	18970	12	3	0.59	0.21	0.42
J03599+5043	18971	10	0	…	…	…
J15541–5613	18972	21	5	−0.11	−0.20	0.63
J19294+1327	18973	17	3	−1.20	0.77	0.32
J16246–4556	18974	27	5	0.09	−0.41	0.43
J16181–5407	18975	14	4	−0.02	−0.41	0.49
J17508–3219	18976	28	7	−0.49	0.18	0.41
J17118–3155	18977	25	4	0.54	−0.21	0.62
J20413+3210	18978	6	0	…	…	…
J07202+0009	18979	26	3	−0.70	0.10	0.35
J17096–2527	18980	23	7	0.20	0.69	0.38
J18007–4146	18981	22	4	0.65	−0.45	0.50
J16482–2959	18982	13	0	…	…	…
J16120–3543	18983	17	1	…	…	…

Notes.
[a] The number of *Chandra* sources detected on the four ACIS-I detector chips.
[b] The number of matches between the *Chandra* detections and the *Gaia* DR2 catalog.
[c] The shifts in the x and y detector coordinate directions in pixels. The conversion is 1 pixel = $0\rlap{.}''492$.
[d] Average residual (in arcseconds) between the *Chandra* and Gaia DR2 sources.

probabilities for *Chandra* sources that are likely candidates to be associated with the IGR sources, we first determine the relative probabilities for all sources using

$$P_{\rm rel} = 1 - e^{-\left(\frac{C_{2-10\,{\rm keV}}}{C_0}\right)^{-1.0} \pi\, \theta_{\rm search}^2}, \qquad (3)$$

where $C_{2-10\,{\rm keV}}$ is the number of counts in the 2–10 keV band, C_0 is an arbitrary normalization constant set so that the brightest sources have $P_{\rm rel}$ values near 1%, and we use −1.0 as the slope of the $\log N - \log S$ since this is the midpoint between the Sugizaki et al. (2001) and Fornasini et al. (2014) values.

Using Equation (3), with $C_0 = 140$, we calculate $P_{\rm rel}$ for all the sources detected in the 15 *Chandra* observations, and these are plotted in Figure 1. This parameter space leads to a large cluster of low count/high $P_{\rm rel}$ field sources and relatively clear separation between this cluster and the *Chandra* sources that are candidates to be counterparts to the IGR sources. For ten of the IGR fields, the most likely counterpart is labeled in Figure 1, and there are two fields with two potential counterparts.

For these 12 sources, Table 4 gives the *Chandra* names and positions, the angular distance from the center of the *INTEGRAL* error circle (θ), the number of ACIS counts in the 0.3–10 keV band, and the hardness ratio. The uncertainties in the positions include systematic and statistical contributions added in quadrature. The determination of the systematic uncertainty is described above (see Table 3). For the statistical contribution, we use Equation (13) from Kim et al. (2007), which uses the number of counts and the angular distance of the source from the *Chandra* aimpoint. The information in Table 4 provides additional information about the likelihood that the *Chandra* sources are the true counterparts to the IGR sources. In particular, J16246a is a questionable counterpart because it is one of the softer sources in the list, and it is well outside the *INTEGRAL* error circle ($\theta = 7\rlap{.}'92$ compared to the error circle radius of $4\rlap{.}'61$). Also, J17508a is questionable since

it is a very soft source, and it is outside the *INTEGRAL* error circle.

3.2. Chandra and INTEGRAL Energy Spectra

For the 12 candidate counterparts, we extracted *Chandra* energy spectra using `specextract`. For the source extraction region, we used a circle with a radius corresponding to 95% encircled energy, which we determined from the PSF map. However, we also checked each source for photon pile-up by making an image for energies greater than 10 keV. For the three sources with evidence for pile-up (J16181, J18007, and J20310), we used an annular source extraction region with an inner radius of 1 pixel to cut out the core of the PSF. We also extracted a background spectrum using the same region used for the photometry. The spectra were rebinned to require a detection in each bin at the 3σ level unless this resulted in fewer than five bins, in which case a 2σ requirement was used.

Using XSPEC (Arnaud 1996), we fit the *Chandra* spectra with an absorbed power-law model, and the parameters are reported in Table 5. We performed the fits by minimizing the C-statistic, and we give the C values and number of degrees of freedom (dof) in Table 5. We use these values along with the variances in C, calculated according to Equations (20)–(22) in Kaastra (2017), to quantify the quality of the fits. The $P_{\rm reject}$ values in Table 5 indicate the probability that an absorbed power law does not provide a good description of the spectrum. The most significant deviations from an absorbed power law are for J16246a, J18007, and J17508a, which have $P_{\rm reject}$ values of 99.7%, 88%, and 84%, respectively. While an absorbed power-law fit is not a formally acceptable model in these cases, the residuals do not show clear evidence for spectral features such as emission lines.

The measured $N_{\rm H}$ values exceed the Galactic column density (see Table 5 for both) for J16181 ($N_{\rm H} = (9 \pm 7) \times 10^{22}$ cm^{-2}; 90% confidence errors are given) and J19294 ($N_{\rm H} = (2.8^{+3.8}_{-2.4}) \times 10^{23}$ cm^{-2}). Several other sources have upper limits on $N_{\rm H}$ that are higher than the Galactic $N_{\rm H}$ (HI4PI Collaboration et al. 2016), but we note that there may be spatial variations in

Table 4
Chandra Candidate Counterparts to IGR Sources

IGR Name	CXOU Name	*Chandra* R.A. (J2000)	*Chandra* Decl. (J2000)	Uncertainty[a] (arcsec)	θ[b]/$\theta_{INTEGRAL}$[c] (arcmin)	ACIS Counts[e]	Hardness[d]
J15038	J150415.7−602123	$15^h04^m15^s70$	−60°21′23″0	0.46	3.69/3.95	259 ± 17	+0.65 ± 0.08
J15541	J155413.0−560932	$15^h54^m13^s09$	−56°09′32″6	0.75	3.54/4.32	44 ± 8	+0.60 ± 0.21
J16181	J161807.7−540612	$16^h18^m07^s74$	−54°06′12″5	0.50	0.04/4.61	253 ± 17	+0.94 ± 0.09
J16246a	J162425.2−460316	$16^h24^m25^s20$	−46°03′16″5	0.67	7.92/4.61	660 ± 27	+0.14 ± 0.04
J16246b	J162430.7−455514	$16^h24^m30^s77$	−45°55′14″1	0.46	1.56/4.61	125 ± 12	+0.62 ± 0.12
J17096	J170950.2−252934	$17^h09^m50^s27$	−25°29′34″4	0.55	2.02/2.73	34 ± 7	+0.12 ± 0.22
J17118	J171135.8−315504	$17^h11^m35^s89$	−31°55′04″5	0.81	3.08/2.84	23 ± 6	+0.30 ± 0.29
J17508a	J175106.8−321827	$17^h51^m06^s85$	−32°18′27″9	0.44	3.21/2.31	713 ± 28	−0.55 ± 0.04
J17508b	J175108.7−322122	$17^h51^m08^s78$	−32°21′22″2	0.48	3.68/2.31	169 ± 14	+0.03 ± 0.09
J18007	J180042.6−414650	$18^h00^m42^s69$	−41°46′50″0	0.51	1.68/3.19	441 ± 22	+0.27 ± 0.05
J19294	J192930.1+132705	$19^h29^m30^s14$	+13°27′05″7	0.39	0.10/3.43	39 ± 7	+1.00 ± 0.27
J20310	J203055.2+383347	$20^h30^m55^s28$	+38°33′47″1	0.35	1.39/4.54	266 ± 17	+0.86 ± 0.09

Notes.
[a] 90% confidence.
[b] The angular distance between the center of the *INTEGRAL* error circle and the source.
[c] The size of the 90% confidence *INTEGRAL* error radius given in Bird et al. (2016).
[d] The hardness is given by $(C_2 − C_1)/(C_2 + C_1)$, where C_2 is the number of counts in the 2–10 keV band and C_1 is the number of counts in the 0.3–2 keV band.
[e] The number of counts, after background subtraction, measured by *Chandra*/ACIS-I in the 0.3–10 keV band.
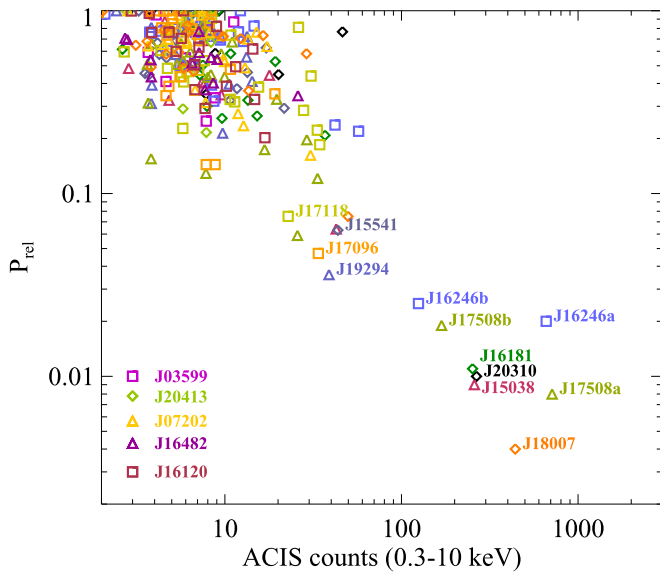
Figure 1. Relative probability of a chance detection (see Equation (3)) vs. the number of ACIS-I counts in the 0.3–10 keV bandpass for all *Chandra* sources detected in the 15 observations of IGR source fields. For the ten fields with candidate counterparts, the source that is least likely to be spurious is labeled with the IGR source name. In two fields (J16246 and J17508), there are two sources that are potential counterparts. The legend in the lower left corner of the plot only includes the five IGR source fields without likely counterparts.

N_H on scales smaller than the angular resolution of the survey. The measured Γ values show that most of the spectra are intrinsically hard. Nine of the sources have photon indices with best-fit values less than or equal to 1.5. J17058a is the softest source with $\Gamma = 3.0 \pm 0.2$. While J17096 and J17508b have $\Gamma = 1.9 \pm 1.3$ and 1.8 ± 0.5, respectively, the errors are relatively large. We use these fits to determine the fluxes in the 2–10 keV band. The "unabsorbed" fluxes are only corrected for the interstellar (Galactic) column density. With

these fluxes, we use

$$P = 1 − e^{−N(>F_{2−10\,keV})\,\pi\,\theta^2_{search}} \qquad (4)$$

to assess the absolute probability of finding a source in the search region (defined by θ_{search}) as bright as the candidate sources. We find $N(>F_{2−10\,keV})$ using the unabsorbed fluxes in Table 5 and Equations (1) and (2), which provides a range of probabilities depending on whether we use the Sugizaki et al. (2001) or the Fornasini et al. (2014) expression. The range of probabilities for each source is given in Table 5. The least likely sources to be chance coincidences are J15038 (0.97%–1.03%), J18007 (1.3%–1.7%), and J20310 (1.5%–1.6%), and the sources that are most likely to be chance coincidences are J15541 (5.4%–10.7%) and J17096 (4.7%–13.7%).

While these are the formal probabilities, we can also obtain information by exploring how the *Chandra* spectra extrapolate into the *INTEGRAL* band. To accomplish this comparison, we produced 2-bin *INTEGRAL* spectra using the fluxes in the Bird et al. (2016) catalog, and refit the *Chandra* spectra jointly with these two higher-energy points. An important caveat is that the *INTEGRAL* fluxes are averages over 7–8 years (up to 2010) while the *Chandra* spectrum is from a single observation in 2017. While the source flux (and possibly spectral shape) may be different for *Chandra* and *INTEGRAL*, we carry out fits without allowing for an offset between the two. Thus, a mismatch between *Chandra* and *INTEGRAL* could be caused by variability or it could indicate that the *Chandra* counterpart is incorrect. Also, for many of the *INTEGRAL* spectra, the flux is dropping between the 20–40 and 40–100 keV energy bands, indicating that the spectrum must change slope between *Chandra* and *INTEGRAL*. For this reason, we use a power law with an exponential cutoff, and fit each spectrum with the XSPEC model tbabs*cutoffpl.

Figure 2 shows the *Chandra*+*INTEGRAL* spectra, and the parameters are given in Table 6. We also used XSPEC for these fits, but we minimized χ^2 instead of C because the *INTEGRAL* points are based on fluxes rather than Poissonian counts. In

Table 5
Chandra Spectral Parameters and Absolute Spurious Probabilities

IGR Name	$N_{\rm H}$[a] $(\times 10^{22}\,{\rm cm}^{-2})$	$N_{\rm H,Galactic}$[b] $(\times 10^{22}\,{\rm cm}^{-2})$	Γ	Absorbed Flux[c] (2–10 keV)	Unabsorbed Flux[d] (2–10 keV)	C/dof	$P_{\rm reject}$[e]	Probability[f]
J15038	<1.0	1.3	0.0 ± 0.3	2.34×10^{-12}	2.35×10^{-12}	25/23	21%	0.97%–1.03%
J15541	<4.3	0.8	1.1 ± 1.1	3.54×10^{-13}	3.78×10^{-13}	5.8/6	⋯	5.4%–10.7%
J16181	9 ± 7	0.5	0.8 ± 1.1	1.27×10^{-12}	1.29×10^{-12}	5.0/7	⋯	2.3%–2.8%
J16246a	0.4 ± 0.3	0.8	1.5 ± 0.2	2.82×10^{-12}	2.89×10^{-12}	90/57	99.7%	3.0%–3.5%
J16246b	2.5 ± 1.6	0.8	1.3 ± 0.7	9.27×10^{-13}	1.04×10^{-12}	16/10	75%	2.9%–3.5%
J17096	<3.6	0.2	1.9 ± 1.3	1.33×10^{-13}	1.45×10^{-13}	5.6/4	31%	4.7%–13.7%
J17118	<4.2	0.3	$1.2^{+1.7}_{-1.1}$	3.22×10^{-13}	3.37×10^{-13}	2.8/2	19%	3.9%–6.4%
J17508a	0.2 ± 0.1	0.5	3.0 ± 0.2	6.22×10^{-13}	6.33×10^{-13}	75/59	84%	1.9%–3.2%
J17508b	0.5 ± 0.5	0.5	1.8 ± 0.5	4.87×10^{-13}	5.00×10^{-13}	17/13	51%	3.1%–5.6%
J18007	<0.14	0.12	0.8 ± 0.2	1.06×10^{-12}	1.06×10^{-12}	23/14	88%	1.3%–1.7%
J19294	28^{+38}_{-24}	0.8	$0.6^{+2.7}_{-2.2}$	5.84×10^{-13}	5.91×10^{-13}	2.1/5	⋯	2.3%–4.0%
J20310	<5.6	1.5	-0.2 ± 0.9	1.95×10^{-12}	2.04×10^{-12}	9.2/9	3%	1.5%–1.6%

Notes.
[a] The errors on the parameters are 90% confidence. The column density is calculated assuming Wilms et al. (2000) abundances and Verner et al. (1996) cross sections.
[b] From the HI4PI survey (HI4PI Collaboration et al. 2016).
[c] In units of erg cm^{-2} s^{-1}.
[d] Only corrected for Galactic absorption.
[e] The probability that an absorbed power law does not provide a good description of the spectrum based on a calculation of the variance of C according to the method described in Kaastra (2017).
[f] Absolute probability that a source of this brightness would be found by chance in the search region.

nearly all cases, the `tbabs*cutoffpl` model provides a reasonably good description of the spectra. One notable exception is J17508a, for which the power-law index is well-constrained by the *Chandra* spectrum to be soft, and the extrapolation into the *INTEGRAL* bandpass is below the *INTEGRAL* fluxes by orders of magnitude. Although this might indicate that J17508b is the correct counterpart, the model does not fit the *Chandra*+*INTEGRAL* spectrum very well for J17508b either ($\chi^2/\nu = 43/14$), and we discuss the case of IGR J17508–3219 further in Section 4.1. J17096 is another case where the `tbabs*cutoffpl` model does not provide a very good fit, but it is clear that a better spectrum is required to understand the cause of the residuals. It is possible that J17096 and J18007 both require an extra spectral component at low energies.

3.3. Optical/IR Identifications

We used the VizieR database to search for optical/IR counterparts to the 12 *Chandra* sources. In seven cases, a *Gaia* DR2 optical source with a position consistent with the *Chandra* position was found, and these are listed in Table 7. Parallax measurements are available for six of the sources. They are negative in two cases, but for the four sources with positive parallaxes, the distance estimates from Bailer-Jones et al. (2018) are $1.1^{+1.5}_{-0.4}$, $2.20^{+0.28}_{-0.22}$, $0.135^{+0.002}_{-0.001}$, and $2.5^{+0.5}_{-0.4}$ kpc for J15038, J16246a, J17508a, and J18007, respectively. Thus, all four sources are Galactic, but it is doubtful that J17508a[13] is the correct counterpart to the IGR source, and J16246a is a questionable counterpart. However, IGR J15038–6021 is a Galactic source at a distance of $1.1^{+1.5}_{-0.4}$ kpc, and IGR J18007–4146 is a Galactic source at a distance of $2.5^{+0.5}_{-0.4}$ kpc.

Six of the twelve *Chandra* sources are present in the AllWISE IR catalog (Cutri et al. 2014), and the *Wide-field Infrared Survey Explorer* (*WISE*) magnitudes at 3.4 μm (*W*1),

4.6 μm (*W*2), 12 μm (*W*3), and 22 μm (*W*4) are given in Table 8. The *WISE* colors *W*3-*W*2 and *W*2-*W*1 have been used to identify AGN and blazars (e.g., Massaro et al. 2012; Secrest et al. 2015; Massaro & D'Abrusco 2016), and we plot these colors for the six sources in Figure 3. It has already been reported by Ursini et al. (2018) that IGR J16181–5407 (and the *Chandra* source J16181) is likely to be an AGN based on its *WISE* colors, and Figure 3 shows that the same criterion leads to IGR J17096–2527 (J17096) being a likely AGN. Figure 3 also shows that the two Galactic sources (based on *Gaia* as discussed above) are far away from the AGN region. J16246b and J19294 are the other two sources in the AllWISE catalog, but we cannot conclude on their nature based on their location in the *WISE* color–color diagram. However, we note that all four AGN candidates (J16181, J17096, J16246b, and J19294) are listed in AllWISE as having spatial profiles that are inconsistent with a point source in at least one photometric band, and the two Galactic sources (J16246a and J17508a) do not show evidence for extension (see Table 8).

In addition to *Gaia* and *WISE*, we found many more optical/IR counterparts to the 12 *Chandra* sources in the VizieR database. Here, we focus on the near-IR information from the Visible and Infrared Survey Telescope for Astronomy (VISTA; Minniti et al. 2010; McMahon et al. 2013; Minniti et al. 2017), the UKIRT Infrared Deep Sky Survey (UKIDSS; Lucas et al. 2008), and the 2 Micron All-Sky Survey (2MASS; Cutri et al. 2003), providing the *J*, *H*, and *K*/*K_s* magnitudes in Table 9 and the *K*/*K_s* images in Figure 4. In the *K*/*K_s* bands, the sources range in brightness with the faintest sources being J17118 ($K_s = 16.97 \pm 0.20$) and J20310 ($K = 16.54 \pm 0.04$) and the brightest sources being J17508a ($K_s = 7.45 \pm 0.03$) and J16246a ($K_s = 11.49 \pm 0.02$). Although J15541 does not appear in the catalogs, Figure 4 shows that it has a faint K_s-band counterpart that is very close to a bright star. In addition, the *K*-band images for J16246b, J19294, and probably J16181 confirm that these sources are extended, making it very likely that they are AGN. It is unclear from the VISTA image

---

[13] Catalog searches also uncovered that this source is the star HD 162186.
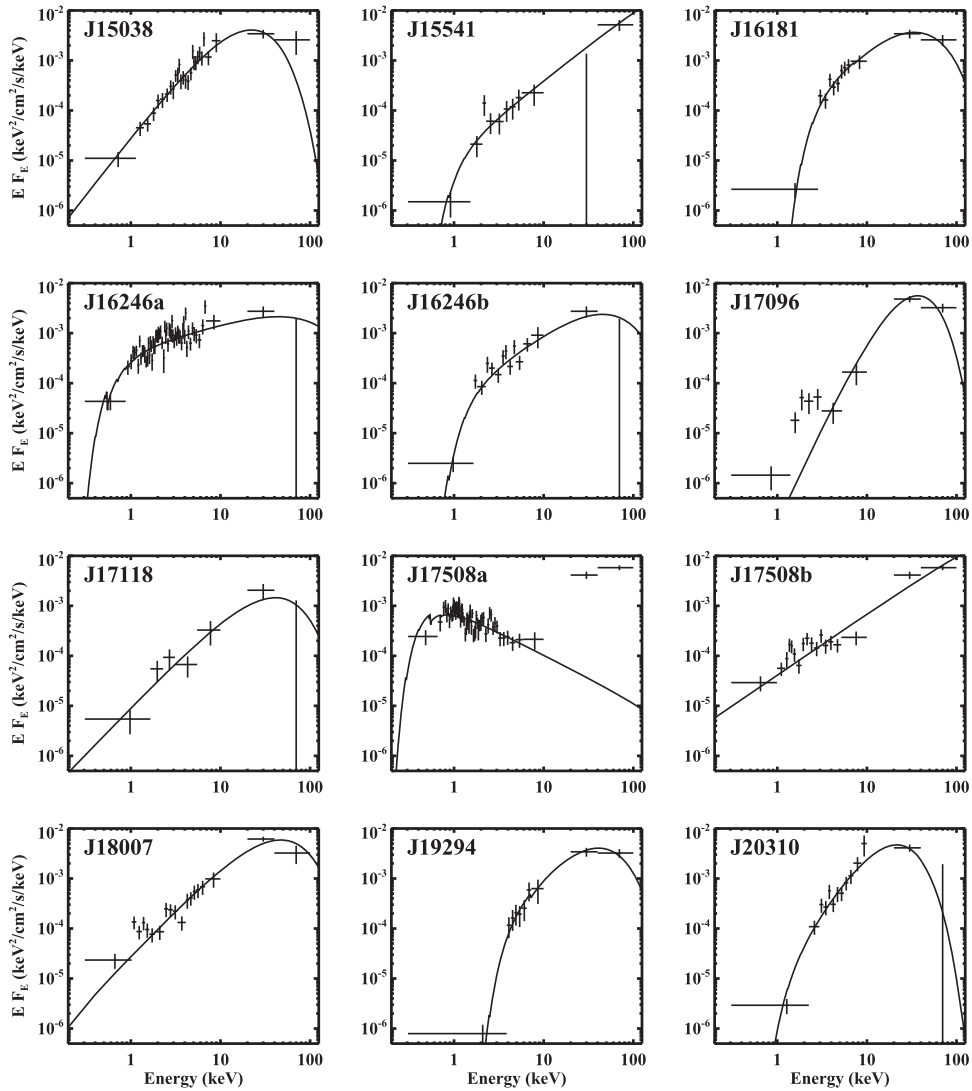
Figure 2. *Chandra* and *INTEGRAL* energy spectra for the 12 candidate counterparts. The two highest energy data points are derived from the fluxes reported in Bird et al. (2016). The best-fit absorbed power law with an exponential high-energy cutoff model (`tbabs*cutoffpl`) is shown. We note that the *INTEGRAL* measurements were made during 2002–2010 while the *Chandra* spectra were obtained in 2017. Thus, it is possible for source variability to cause poor fits in some cases.

whether J17096 is extended, and it is also classified as being a star in the VISTA catalog (see Table 9); however, we still consider it to be likely that J17096 is an AGN based on the *WISE* information. For J20310, the *K*-band image from UKIDSS may show some extension, and the source is classified as being a galaxy in the UKIDSS catalog.

In summary, the parallax measurements for J15038, J16246a, J17058a, and J18007 show that these four *Chandra* sources are Galactic, and the K/K_s images (Figure 4) are consistent with this in that they do not show evidence that these sources are extended. Based on the sources being extended and/or the *WISE* colors, J16181, J16246b, J17096, and J19294 are AGN, and J20310 is an AGN candidate based on the UKIDSS information. We discuss the nature of the remaining three sources (J15541, J17118, and J17058b) below.

4. Discussion

The main goal of this work is to determine the nature of the 15 IGR sources (see Table 2) by determining the most likely *Chandra* counterparts and then using the *Chandra* localizations

along with information in online catalogs and databases to classify the sources. There are two IGR sources with two possible *Chandra* counterparts: IGR J16246−4556 and IGR J17508−3219; and we discuss those cases first. Then, we consider the two sources definitively classified as being Galactic: IGR J18007−4146 and IGR J15038−6021. After that, we discuss the unclassified sources with *Chandra* counterparts: IGR J15541−5613 and IGR J17118−3155 and then the cases without likely *Chandra* counterparts.

4.1. IGR Sources with Two Candidate Chandra Counterparts

For IGR J16246−4556, the two candidate *Chandra* counterparts that we are considering are J16246a (3.0%–3.5%) and J16246b (2.9%–3.5%). Both of them have hard spectra ($\Gamma = 1.5 \pm 0.2$ and 1.3 ± 0.7, respectively, from the *Chandra*-only fits) that are consistent with the *INTEGRAL* fluxes (see Figure 2), and their spurious probabilities are the same because J16246a is about three times brighter, while J16246b is only $1.'56$ from the center of the *INTEGRAL* error circle, while $\theta = 7.'92$ for J16246a. Given that the 90% confidence *INTEGRAL* radius is $4.'61$, an

Table 6
Chandra+INTEGRAL Spectral Parameters

IGR Name	$N_{\rm H}$[a] $(\times 10^{22}\,{\rm cm}^{-2})$	Γ	$E_{\rm fold}$ (keV)	Unabsorbed Flux[b] (0.3–100 keV)	χ^2/dof[c]
J15038	<1.0	$-0.3^{+0.6}_{-0.3}$	10^{+8}_{-2}	1.11×10^{-11}	22/24
J15541	<2.4	$0.6^{+0.2}_{-0.6}$	>36	1.07×10^{-11}	5/7
J16181	8 ± 5	0.3 ± 0.7	20^{+33}_{-8}	1.10×10^{-11}	5/8
J16246a	0.3 ± 0.3	1.4 ± 0.3	>22	1.01×10^{-11}	86/58
J16246b	1.4 ± 1.3	0.6 ± 0.7	>12	7.6×10^{-12}	18/11
J17096[c]	0.0	-2.0	9	1.15×10^{-11}	21/5
J17118	<1.4	$0.2^{+1.1}_{-0.7}$	>8	4.2×10^{-12}	6/3
J17508a[c]	0.15	2.9	500	2.2×10^{-12}[d]	192/60
J17508b	<0.8	0.8 ± 0.1	>179	1.35×10^{-11}	43/14
J18007	<0.12	0.1 ± 0.3	25^{+13}_{-8}	1.67×10^{-11}	43/15
J19294	24^{+21}_{-14}	-0.1 ± 0.9	20^{+42}_{-8}	1.08×10^{-11}	2/6
J20310	<4.6	-0.9 ± 1.1	7^{+10}_{-3}	1.14×10^{-11}	9/10

Notes.
[a] The errors on the parameters are 90% confidence. The column density is calculated assuming Wilms et al. (2000) abundances and Verner et al. (1996) cross sections.
[b] In units of erg cm^{-2} s^{-1}, and corrected for Galactic absorption.
[c] The quality of the fit does not allow for errors to be calculated. The `tbabs*cutoffpl` does not provide a good description of the spectrum.
[d] This is the flux for the model shown in Figure 2, which is well below the *INTEGRAL* measurements.

Table 7
Gaia Identifications

IGR Name	*Gaia* Number (in DR2)	Separation[a] (arcsec)	*G*-magnitude	Parallax (milliarcsecond)	Distance[b] (kpc)
J15038	5876459780108921216	0.072	19.055 ± 0.006	1.09 ± 0.37	$1.08^{+1.53}_{-0.42}$
J15541	5836092447721411584	0.245	20.392 ± 0.019	-6.92 ± 1.87	$\cdots$
J16246a	5942431027538084608	0.463	15.494 ± 0.003	0.43 ± 0.05	$2.20^{+0.28}_{-0.22}$
J17096	4112378173142821248	0.049	19.360 ± 0.006	-0.52 ± 0.43	$\cdots$
J17508a	4043524762244704000	0.240	9.027 ± 0.001	7.33 ± 0.04	$0.135^{+0.002}_{-0.001}$
J17508b	4043518508770139648	0.383	18.884 ± 0.018	$\cdots$	$\cdots$
J18007	6725376279628784384	0.331	16.009 ± 0.006	0.38 ± 0.06	$2.49^{+0.49}_{-0.36}$

Notes.
[a] The angular separation between the *Chandra* position and the *Gaia* catalog position.
[b] From Bailer-Jones et al. (2018).

Table 8
WISE Identifications

IGR Name	AllWISE Name	Separation[a] (arcsec)	W1	W2	W3	W4	ex[b]
J16181	J161807.75–540612.3	0.21	11.29 ± 0.04	10.12 ± 0.02	7.55 ± 0.02	4.97 ± 0.04	1
J16246a	J162425.20–460316.7	0.28	11.35 ± 0.03	11.37 ± 0.02	11.88 ± 0.38	$\cdots$	0
J16246b	J162430.78–455514.4	0.35	10.70 ± 0.02	10.52 ± 0.02	8.74 ± 0.04	6.58 ± 0.07	1
J17096	J170950.25–252934.7	0.41	13.61 ± 0.04	12.54 ± 0.03	9.40 ± 0.06	6.78 ± 0.14	1
J17508a	J175106.84–321827.8	0.11	7.41 ± 0.03	7.48 ± 0.02	7.29 ± 0.02	6.52 ± 0.09	0
J19294	J192930.14+132705.9	0.32	12.56 ± 0.03	12.28 ± 0.03	9.71 ± 0.05	7.38 ± 0.12	1

Notes.
[a] The angular separation between the *Chandra* position and the AllWISE catalog position.
[b] A "0" indicates that the source is consistent with being a point source, and a "1" indicates that the profile is not well-described as a point source in at least one photometric band.

offset of 7.′92 corresponds to the 3σ error radius; thus, it is unlikely that the source would be offset by this much, and we note that none of the other *Chandra* counterparts have values of θ that are more than 3.′7 (see Table 4). While J16246a may be an interesting source and worthy of attention, we identify J16246b with IGR J16246–4556, making this IGR source an AGN. The fact that J16246b is a galaxy is confirmed by the VizieR search, which shows a detection of the source in the Parkes HI zone of avoidance survey (Staveley-Smith et al. 2016). It is the galaxy HIZOA J1624-45B, which has a distance of 78.7 Mpc.

Table 9
VISTA, 2MASS, and UKIDSS Identifications

IGR Name	Catalog	Source (arcsec)	Separation[a]	J	H	K/K_s	Class[b]
J15038	VISTA	VVV J150415.72–602122.87	0.230	16.13 ± 0.02	15.48 ± 0.02	$K_s = 15.03 \pm 0.02$	−1
J15541	⋯	⋯	⋯	⋯	⋯	See Figure 4.	⋯
J16181	2MASS	2MASS J16180771–5406122	0.365	⋯	14.09 ± 0.04	$K_s = 12.85 \pm 0.06$	⋯
J16246a	2MASS	2MASS J16242520–4603169	0.409	12.61 ± 0.02	11.78 ± 0.02	$K_s = 11.49 \pm 0.02$	⋯
J16246b	2MASS	2MASS J16243080–4555144	0.519	14.31 ± 0.10	12.98 ± 0.11	$K_s = 12.19 \pm 0.08$	⋯
J17096	VISTA	VHS 472814537075	0.135	17.06	⋯	$K_s = 15.81$	−1
J17118	VISTA	VVV J171135.91–315503.61	0.929	18.64 ± 0.28	18.00 ± 0.33	$K_s = 16.97 \pm 0.20$	−2
J17508a	2MASS	2MASS J17510684–3218276	0.054	7.89 ± 0.02	7.59 ± 0.04	$K_s = 7.45 \pm 0.03$	⋯
J17508b	VISTA	VVV J175108.76–322122.39	0.306	14.73 ± 0.02	13.63 ± 0.02	$K_s = 13.17 \pm 0.01$	−1
J18007	VISTA	VVV J180042.71–414650.23	0.339	15.60 ± 0.01	15.34 ± 0.01	$K_s = 15.31 \pm 0.03$	−1
J19294	UKIDSS	UGPS J192930.11+132705.7	0.372	16.30 ± 0.01	15.09 ± 0.01	$K = 14.32 \pm 0.01$	1
J20310	UKIDSS	UGPS J203055.29+383347.1	0.180	18.83 ± 0.05	17.30 ± 0.02	$K = 16.54 \pm 0.04$	1

Notes.
[a] The angular separation between the *Chandra* position and the catalog position.
[b] The classification based on the spatial profile, where −2 is a probable star, −1 is a star with probability $\geqslant 90\%$, and 1 is a galaxy with probability $\geqslant 90\%$.
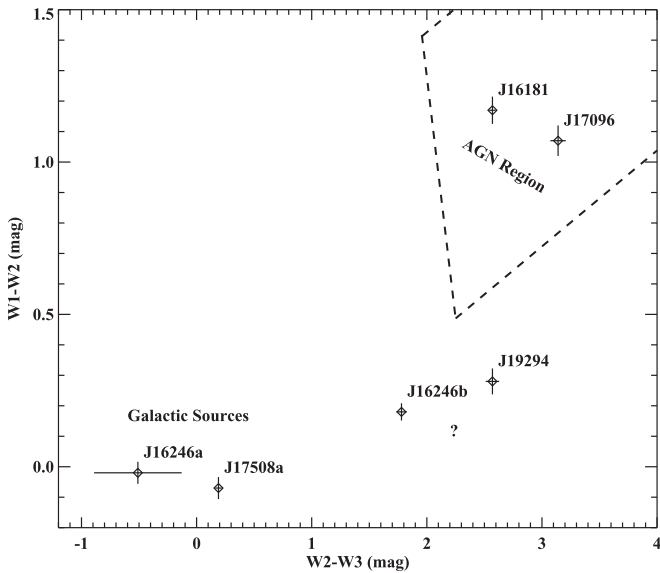
Figure 3. Near-IR colors measured for six of the IGR sources by *WISE*. *W*1, *W*2, and *W*3 are 3.4 μm, 4.6 μm, and 12 μm, respectively. Based on *Gaia* distances, J16246a and J17508a are Galactic sources (this work). J16181 and J17096 are in a region commonly populated by AGN (Secrest et al. 2015; Ursini et al. 2018). The region originally defined by Mateos et al. (2012) is indicated by the dashed lines.

Based on the *Chandra* and *INTEGRAL* spectrum, the unabsorbed 0.3–100 keV flux is 7.7×10^{-12} erg cm^{-2} s^{-1}, making the luminosity 5.7×10^{42} erg s^{-1}.

IGR J17508–3219 has the two candidate *Chandra* counterparts J17508a and J17508b. Both are outside the 2′.31 (90% confidence) *INTEGRAL* error circle with $\theta = 3'.21$ and $3'.68$ for J17508a and J17508b, respectively. As mentioned earlier, J17508a is a soft source ($\Gamma = 3.0 \pm 0.2$) and is inconsistent with the *INTEGRAL* fluxes (see Figure 2); thus, we rule out J17508a as the counterpart. For J17508b, the VizieR search shows that it is coincident with the source OGLE-BLG-DN-0184, which is a dwarf nova (DN) non-magnetic CV with a few optical outbursts per year. The typical outburst duration for OGLE-BLG-DN-0184 is 13.1 days where the optical brightness increases from $I = 17.5$ to 15.7 (Mróz et al. 2015). Although 56 CVs appear in the Bird et al. (2016) catalog,

nearly all of the CVs that have been classified are IPs or polars, which have highly magnetized white dwarfs. However, some non-magnetic DNe can produce hard X-ray emission above at least 14 keV (Mukai 2017), and J17508b has a relatively hard spectrum with $\Gamma = 1.8 \pm 0.5$. Although we consider J17508b to be a possible counterpart, we also note that Landi et al. (2017) reported on a *Swift*/XRT observation where a third source (#1 in the work of Landi) was detected within the *INTEGRAL* error circle with a 2–10 keV flux of 8×10^{-13} erg cm^{-2} s^{-1} and $\Gamma = 0.6 \pm 0.8$. Landi source #1 is not detected in the *Chandra* observation, and the upper limit on the 2–10 keV flux is approximately an order of magnitude lower than the flux detected by *Swift*. If Landi source #1 is the true counterpart of IGR J17508–3219, this level of variability is surprising given that it is noted to be a persistent source in Bird et al. (2016). Given that Landi source #1 is a hard source within the *INTEGRAL* error circle, it must be considered as a strong candidate, but we also cannot rule out the possibility that J17508b also contributes to the flux seen by *INTEGRAL*.

4.2. Galactic Source IGR J18007–4146

IGR J18007–4146 is associated with an *XMM-Newton* slew source XMMSL1 J180042.8–414651, and the source was also detected by *Swift*/XRT (Landi et al. 2017). Multiple optical/IR sources are consistent with the *XMM* and *Swift* localizations (Landi et al. 2017), but the *Chandra* position for CXOU J180042.6–414650 that we report allows for a unique identification in multiple optical/IR surveys, including VISTA and *Gaia*. It is the VISTA source VVV J180042.71–414650.23, and the *Gaia* counterpart has a parallax distance measurement of $2.5^{+0.5}_{-0.4}$ kpc. The *Chandra* energy spectrum is a very hard power law ($\Gamma < 1$), and combining it with the *INTEGRAL* fluxes indicates that the spectrum turns over at around 25 keV. The 0.3–100 keV flux is $(1.67 \pm 0.35) \times 10^{-11}$ erg cm^{-2} s^{-1}, and this corresponds to a luminosity of $(1.2 \pm 0.5) \times 10^{34}$ erg s^{-1}. Known Galactic source types that may match these properties are CV/IPs or accreting pulsars, which are most often found in HMXBs.

The origin of the optical/IR emission is unclear. If the source is a CV/IP, the emission would be a combination of an accretion disk and a star. Most CV/IPs have late-type stars, and the accretion disk dominates. If the source is an HMXB, then the
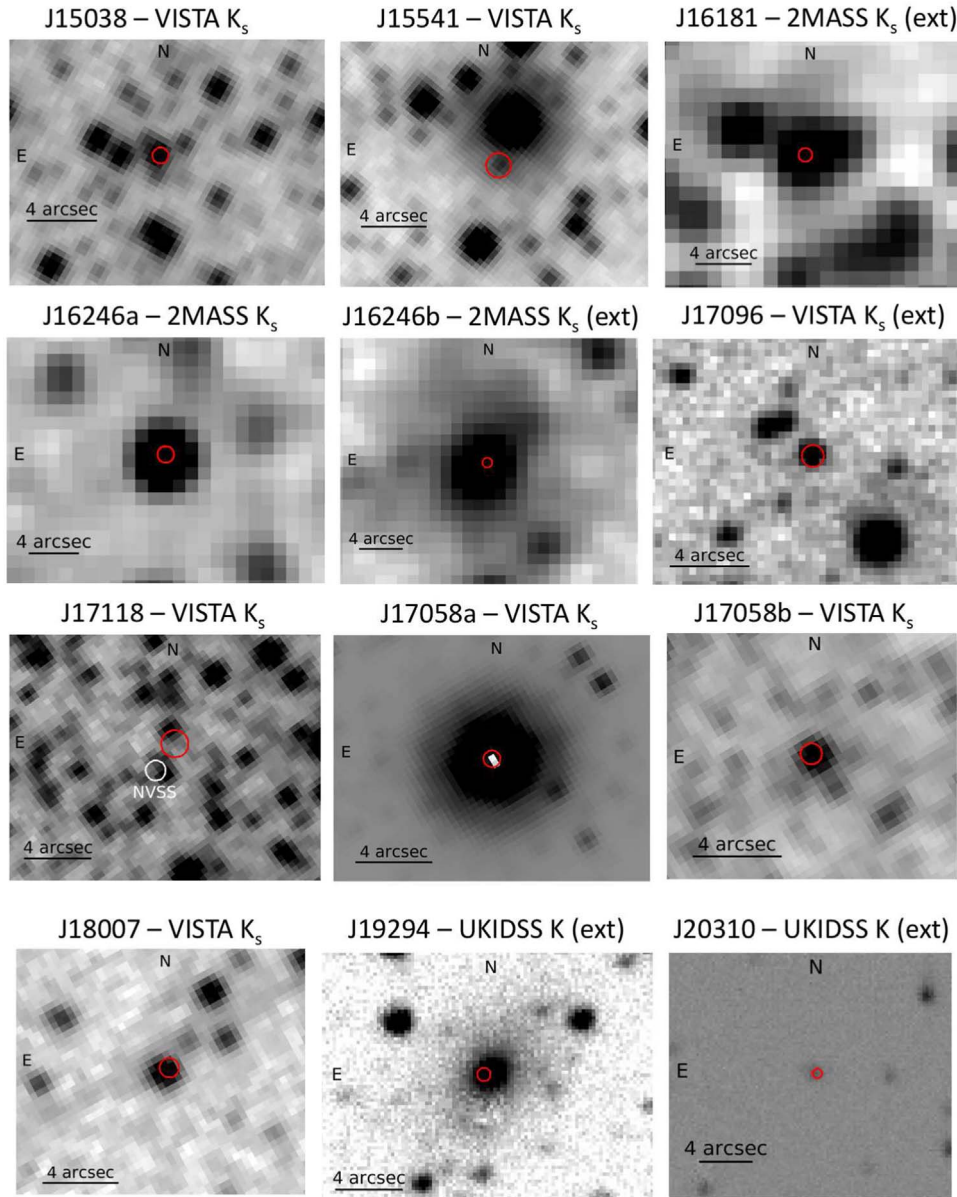
Figure 4. K or K_s band images from the VISTA, 2MASS, and UKIDSS surveys for the 12 candidate counterparts. The red circles indicate the *Chandra* positions (90% confidence). The sources that are extended (i.e., with spatial distributions that are not point-like; see Table 9) are J16181, J16246b, J17096, J19294, and J20310 and are indicated with "(ext)" in the titles above the images.

high-mass star (O- or B-type) would dominate. In either case, the emission is thermal, and we can estimate the temperature using the near-IR colors. The X-ray spectrum does not show evidence for any absorption, with a 90% confidence upper limit of $N_{\rm H} < 1.2 \times 10^{21}\,{\rm cm}^{-2}$, corresponding to $A_V < 0.54$ (Güver & Özel 2009). Using the VISTA near-IR magnitudes and the Cardelli et al. (1989) extinction law, the dereddened magnitudes are $J = 15.45$–15.60 and $H = 15.34$–15.24. Thus, J–H is between 0.21 and 0.26, which corresponds to a temperature of $\sim$6500 K. If this was a stellar temperature, it would correspond to an F5V spectral type, which has $M_J = 2.7$. For IGR J18007–4146, if the extinction is zero, then $M_J = 3.6 \pm 0.4$, and if the extinction is at the maximum value ($A_J = 0.15$), it would be $M_J = 3.5 \pm 0.4$, and these values correspond to a spectral type of G2V. To accommodate a F5V star, the source distance would need to be $\sim$3.5 kpc, which is higher than the Bailer-Jones et al. (2018) value at the 2σ level. Regardless of whether the distance could be as high

as 3.5 kpc, these calculations show that IGR J18007–4146 does not harbor a high-mass O- or B-type star. In fact, if there is a significant contribution to the optical/IR emission from an accretion disk, it is possible that the source is a binary with a late-type star. Given the possible classifications mentioned above (a CV/IP or an HMXB), a CV/IP is strongly favored. However, follow-up optical spectroscopy is needed for confirmation.

4.3. Galactic Source IGR J15038–6021

IGR J15038–6021 was also previously reported as a *Swift*/ XRT source by Landi et al. (2017), but the X-ray localization was not adequate to identify a unique optical/IR counterpart. The detection of this source by *Chandra* as CXOU J150415.7–602123 provides the unique optical/IR identification with the VISTA source VVV 150415.72–602122.87 as well as a *Gaia* source, which provides a parallax distance of $1.1^{+1.5}_{-0.4}$ kpc. The X-ray energy spectrum is slightly harder than IGR J18007–4146, and

the 0.3–100 keV flux is $(1.11 \pm 0.28) \times 10^{-11}$ erg cm^{-2} s^{-1}, corresponding to a luminosity of $(1.6^{+4.4}_{-1.2}) \times 10^{33}$ erg s^{-1}. This suggests the same possibilities for classifications mentioned above: HMXB or CV/IP.

We carry out a similar calculation as for IGR J18007–4146 using the J and H magnitudes along with the *Gaia* distance. Even though IGR J15038–6021 is closer than IGR J18007–4146, it is in the Galactic plane ($b = -1°57$ compared to $b = -9°12$ for IGR J18007–4146), and although the best-fit value for $N_{\rm H}$ is zero for both sources, the upper limit for IGR J15038–6021 is higher ($N_{\rm H} < 1.0 \times 10^{22}$ cm^{-2}). This limit on the column density corresponds to $A_V < 4.52$ (Güver & Özel 2009), and we calculate dereddened magnitudes of $J = 14.86$–16.13 and $H = 14.62$–15.48, giving a range of $J–H$ values between 0.24 and 0.65 and a range of temperatures between 4000 and 6500 K. This allows for a range of stellar spectral types between K5V and F5V.

Turning to the measurement of the absolute magnitude, assuming the *Gaia* distance ($1.1^{+1.5}_{-0.4}$ kpc), if there is no extinction, then $M_J = 5.9^{+0.8}_{-3.0}$, and if the extinction is maximal ($A_J = 1.27$), then $M_J = 4.7^{+0.8}_{-3.0}$. If the errors are included, these absolute magnitudes correspond to spectral types between K5V and A5V. Although this is a large range, it does not cover O and B stars. However, in this case, we must treat the *Gaia* distance with some caution because the *Gaia* DR2 catalog indicates that the astrometric noise for this source is significant. Thus, we performed an additional calculation and found that the distance would need to be 10 kpc to move the absolute magnitude of IGR J15038–6021 into the late B-type range. Thus, based on both the temperatures derived above and the fact that it is very unlikely for the true distance to be larger than the *Gaia* measurement by 6σ, we conclude that IGR J15038–6021 is likely to be a CV/IP.

4.4. Unclassified Sources with Chandra Counterparts

Although our candidate *Chandra* counterpart to IGR J15541–5613, CXOU J155413.0–560932, has a relatively high spurious probability of 5.4%–10.7%, Figure 2 shows that the spectrum rises throughout the *Chandra* band with $\Gamma = 1.1 \pm 1.1$, and the source is also unusual for a Galactic source in having a higher flux in the 40–100 keV band than in the 20–40 keV band. This suggests that IGR J15541–5613 is more likely to be an AGN than a Galactic source. It is conceivable that the high point in the *Chandra* spectrum at ∼2 keV is a redshifted iron line, but the statistical significance of the putative line is low. Also, the implied redshift is $z \sim 2$, and this would indicate a very luminous and rare AGN. Figure 4 shows that, with the bright nearby source, obtaining an optical or near-IR spectrum of IGR J15541–5613 will be challenging, but it may be possible.

For our candidate *Chandra* counterpart to IGR J17118–3155, CXOU J171135.8–315504, a search of the SIMBAD database shows a possible Very Large Array radio counterpart, NVSS J171135–315506. This radio source is quite bright, and is seen in several radio surveys (Douglas et al. 1996; Condon et al. 1998; Murphy et al. 2007; Intema et al. 2017): the Giant Metrewave Radio Telescope/GMRT (1496 mJy at 150 MHz); the Texas Survey/TXS (606 mJy at 365 MHz); the Molonglo Galactic Plane Survey/MGPS-2 (225 mJy at 843 MHz); and the NRAO VLA Sky Survey/NVSS (165 mJy at 1420 MHz). However, considering the best estimates for the radio positions, only the TXS position is within the *Chandra* error circle with the other sources being $2''3 \pm 2''0$ (GMRT), $1''5 \pm 1''6$ (MGPS-2), and $2''0 \pm 0''6$ (NVSS) away from the center of the *Chandra*

error circle. The NVSS error circle is shown on the VISTA K_s image (Figure 4), and it is clear that the error region does not overlap with *Chandra*. We also plotted the NVSS error circle on the *Chandra*/ACIS image, and none of the 23 ACIS counts fall within the NVSS error circle. We repeated this analysis without the $0''3$ position registration shift (see Table 3), and there are still no ACIS counts in the NVSS error circle. While it would be a somewhat surprising coincidence for these two relatively unusual sources to be as close to each other as they are and not be associated, our analysis does not support an association between the two.

4.5. IGR Sources without Likely Chandra Counterparts

Although *Chandra* sources were detected in the *INTEGRAL* error circles for all 15 IGR sources included in this work, there were five cases (IGR J03599+5043, IGR J07202+0009, IGR J16482–2959, IGR J16120–3543, and IGR J20413+3210) where the *Chandra* sources all had relatively high probability of being chance detections of field sources. The *Chandra* sources in *INTEGRAL* error circles of these five IGR sources with the lowest values of $P_{\rm rel}$ are 24.9%, 27.9%, 37.0%, 20.2%, and 21.6%, respectively. We searched the VizieR database to check whether any of the *Chandra* sources have a classified counterpart, and the source with $P_{\rm rel} = 20.2\%$ (CXOU J161147.0–354634)[14] is a *WISE* source (AllWISE J161147.06–354635.0) that has been classified as an AGN based on its *WISE* colors (Secrest et al. 2015). The 2–10 keV X-ray flux is $(9.9^{+6.5}_{-7.1}) \times 10^{-14}$ erg cm^{-2} s^{-1}. While this may still be a spurious identification, we consider the CXOU/AllWISE source to be a candidate counterpart.

Within the *INTEGRAL* error circles of the other four IGR sources (IGR J03599+5043, IGR J07202+0009, IGR J16482–2959, and IGR J20413+3210), the *Chandra* sources with the lowest $P_{\rm rel}$ values have between five and seven counts in the 2–10 keV band. Taking seven counts (0.0014 c s^{-1}) as the upper limit, we can use PIMMS[15] to determine the approximate flux upper limit. If we assume $\Gamma > 0$ and $N_{\rm H} = 10^{22}$ cm^{-2}, we find a flux limit of $< 7 \times 10^{-14}$ erg cm^{-2} s^{-1} in the 2–10 keV energy band. There are several possible interpretations for these IGR sources. When similar results have previously been obtained for other IGR sources, Tomsick et al. (2016a) consider that those IGR sources may be variable or may have hard spectra (either due to high column densities or hard power-law slopes). It is notable that IGR J03599+5043, IGR J07202+0009, IGR J16482–2959, and IGR J20413+3210 are marked as being variable in Bird et al. (2016; see Table 1). Another possibility is that these IGR sources are spurious, but the *INTEGRAL* signal-to-noise values are between 5.9 and 7.5 (Table 1).

5. Summary and Conclusions

Our final results for each of the 15 IGR sources are summarized in Table 10, including the name of the *Chandra* counterpart or upper limit on the X-ray flux, our conclusion about the source type, and the main evidence we use to come to our conclusion. IGR J15038–6021 and IGR J18007–4146 are strong CV/IP candidates, and this could be confirmed in the future with optical or near-IR spectroscopy. We definitively

---

[14] The *Chandra* position is R.A. = $16^{\rm h}11^{\rm m}47^{\rm s}04$, decl. = $-35°46'34''9$, equinox 2000.0 with a 90% confidence position uncertainty of $0''90$.
[15] See https://asc.harvard.edu/toolkit/pimms.jsp.

Table 10
Summary of Results

IGR Name	*Chandra* Counterpart or 2–10 keV Flux Limit	Source Type	Evidence
J03599+5043	$<1.5 \times 10^{-13}$	…	…
J07202+0009	$<1.4 \times 10^{-13}$	…	…
J15038−6021	CXOU J150415.7−602123	CV/IP?	*Gaia* distance, near-IR magnitudes, X-ray spectrum
J15541−5613	CXOU J155413.0−560932	AGN?	X-ray spectrum
J16120−3543	CXOU J161147.0−354634?	AGN?	*WISE* colors
J16181−5407	CXOU J161807.7−540612	AGN	*WISE* colors and extended in near-IR
J16246−4556	CXOU J162430.7−455514	AGN	Extended in near-IR
J16482−2959	$<1.5 \times 10^{-13}$	…	…
J17096−2527	CXOU J170950.2−252934	AGN	*WISE* colors and extended in near-IR
J17118−3155	CXOU J171135.8−315504	?	?
J17508−3219	CXOU J175108.7−322122?	?[a]	?
J18007−4146	CXOU J180042.6−414650	CV/IP?	*Gaia* distance, near-IR magnitudes, X-ray spectrum
J19294+1327	CXOU J192930.1+132705	AGN	Extended in near-IR
J20310+3835	CXOU J203055.2+383347	AGN?	Likely extended in near-IR
J20413+3210	$<1.5 \times 10^{-13}$	…	…

Note.
[a] While CXOU J175108.7−322122 is classified as a Dwarf Nova and may be the counterpart, source #1 detected in the field by *Swift* (Landi et al. 2017) is a variable source that is another possible counterpart.

classify four IGR sources as AGN and three as AGN candidates. This relatively high fraction of AGN may not be too surprising as the new IGR sources found recently are, on average, fainter than the IGR sources found earlier in the mission. We also note that the plot of near-IR colors measured by *WISE* (Figure 3), which has been used to identify AGN, may be a useful tool for identifying Galactic sources as well. Finally, although we detected likely *Chandra* counterparts to IGR J17508−3219 and IGR J17118−3155, the classifications are unclear. Additional X-ray observations of IGR J17508−3219 may be useful to determine if the true counterpart is CXOU J175108.7−322122 or the Landi et al. (2017) *Swift* source. For IGR J17118−3155, the uncertainty on the X-ray position could be reduced with a longer *Chandra* observation with the source on-axis.

ORCID iDs

John A. Tomsick ● https://orcid.org/0000-0001-5506-9855
Arash Bodaghee ● https://orcid.org/0000-0002-7315-3732
Maïca Clavel ● https://orcid.org/0000-0003-0724-2742
Francesca M. Fornasini ● https://orcid.org/0000-0002-9286-9963
Jeremy Hare ● https://orcid.org/0000-0002-8548-482X
Roman Krivonos ● https://orcid.org/0000-0003-2737-5673
Farid Rahoui ● https://orcid.org/0000-0001-7655-4120
Jerome Rodriguez ● https://orcid.org/0000-0002-4151-4468

References

Arnaud, K. A. 1996, in ASP Conf. Ser. 101, Astronomical Data Analysis Software and Systems V, ed. G. H. Jacoby & J. Barnes (San Francisco, CA: ASP), 17
Bailer-Jones, C. A. L., Rybizki, J., Fouesneau, M., Mantelet, G., & Andrae, R. 2018, AJ, 156, 58
Bird, A. J., Bazzano, A., Bassani, L., et al. 2010, ApJS, 186, 1
Bird, A. J., Bazzano, A., Malizia, A., et al. 2016, ApJS, 223, 15
Bonnet-Bidaud, J. M., de Martino, D., Falanga, M., Mouchet, M., & Masetti, N. 2007, A&A, 473, 185
Cardelli, J. A., Clayton, G. C., & Mathis, J. S. 1989, ApJ, 345, 245
Chaty, S., Rahoui, F., Foellmi, C., et al. 2008, A&A, 484, 783
Coleiro, A., Chaty, S., Zurita Heras, J. A., Rahoui, F., & Tomsick, J. A. 2013, A&A, 560, A108
Condon, J. J., Cotton, W. D., Greisen, E. W., et al. 1998, AJ, 115, 1693
Cutri, R. M., Skrutskie, M. F., van Dyk, S., et al. 2003, 2MASS All Sky Catalog of Point Sources, NASA/IPAC Infrared Science Archive, http://irsa.ipac.caltech.edu/applications/Gator/
Cutri, R. M., et al. 2014, yCat, 2328, 0
Douglas, J. N., Bash, F. N., Bozyan, F. A., Torrence, G. W., & Wolfe, C. 1996, AJ, 111, 1945
Fornasini, F. M., Tomsick, J. A., Bodaghee, A., et al. 2014, ApJ, 796, 105

Fortin, F., Chaty, S., Coleiro, A., Tomsick, J. A., & Nitschelm, C. H. R. 2018, A&A, 618, A150

Fruscione, A., McDowell, J. C., Allen, G. E., et al. 2006, Proc. SPIE, 6270, 62701V

Gaia Collaboration, Brown, A. G. A., Vallenari, A., et al. 2018, A&A, 616, A1

Garmire, G. P., Bautz, M. W., Ford, P. G., Nousek, J. A., & Ricker, G. R. 2003, Proc. SPIE, 4851, 28

Güver, T., & Özel, F. 2009, MNRAS, 400, 2050

HI4PI Collaboration, Ben Bekhti, N., Flöer, L., et al. 2016, A&A, 594, A116

Intema, H. T., Jagannathan, P., Mooley, K. P., & Frail, D. A. 2017, A&A, 598, A78

Kaastra, J. S. 2017, A&A, 605, A51

Kim, M., Kim, D.-W., Wilkes, B. J., et al. 2007, ApJS, 169, 401

Krivonos, R. A., Tsygankov, S. S., Mereminskiy, I. A., et al. 2017, MNRAS, 470, 512

Landi, R., Bassani, L., Bazzano, A., et al. 2017, MNRAS, 470, 1107

Landi, R., Bassani, L., Dean, A. J., et al. 2009, MNRAS, 392, 630

Landi, R., Bassani, L., Masetti, N., et al. 2012, ATel, 4233

Lucas, P. W., Hoare, M. G., Longmore, A., et al. 2008, MNRAS, 391, 136

Masetti, N., Parisi, P., Palazzi, E., et al. 2013, A&A, 556, A120

Massaro, F., & D'Abrusco, R. 2016, ApJ, 827, 67

Massaro, F., Paggi, A., D'Abrusco, R., & Tosti, G. 2012, ApJ, 750, L35

Mateos, S., Alonso-Herrero, A., Carrera, F. J., et al. 2012, MNRAS, 426, 3271

Matt, G., & Guainazzi, M. 2003, MNRAS, 341, L13

McMahon, R. G., Banerji, M., Gonzalez, E., et al. 2013, Msngr, 154, 35

Minniti, D., Lucas, P. & VVV Team 2017, yCat, 2348, 0

Minniti, D., Lucas, P. W., Emerson, J. P., et al. 2010, NewA, 15, 433

Mróz, P., Udalski, A., Poleski, R., et al. 2015, AcA, 65, 313

Mukai, K. 2017, PASP, 129, 062001

Murphy, T., Mauch, T., Green, A., et al. 2007, MNRAS, 382, 382

Negueruela, I., Smith, D. M., Reig, P., Chaty, S., & Torrejón, J. M. 2006, in ESA SP-604: The X-ray Universe 2005, ed. A. Wilson (Noordwijk: ESA), 165

Pavan, L., Bordas, P., Puehlhofer, G., et al. 2014, A&A, 562, A122

Pavan, L., Bozzo, E., Pühlhofer, G., et al. 2011, A&A, 533, A74

Prusti, T., de Bruijne, J. H. J., Brown, A. G. A., et al. 2016, A&A, 595, A1

Romano, P., Krimm, H. A., Palmer, D. M., et al. 2014, A&A, 562, A2

Secrest, N. J., Dudik, R. P., Dorland, B. N., et al. 2015, ApJS, 221, 12

Sguera, V., Bazzano, A., Bird, A. J., et al. 2006, ApJ, 646, 452

Staveley-Smith, L., Kraan-Korteweg, R. C., Schröder, A. C., et al. 2016, AJ, 151, 52

Sugizaki, M., Mitsuda, K., Kaneda, H., et al. 2001, ApJS, 134, 77

Tomsick, J. A., Bodaghee, A., Chaty, S., et al. 2012a, ApJ, 754, 145

Tomsick, J. A., Bodaghee, A., Rodriguez, J., et al. 2012b, ApJL, 750, L39

Tomsick, J. A., Chaty, S., Rodriguez, J., et al. 2006, ApJ, 647, 1309

Tomsick, J. A., Chaty, S., Rodriguez, J., Walter, R., & Kaaret, P. 2009, ApJ, 701, 811

Tomsick, J. A., Kalemci, E., Kaaret, P., et al. 2008, ApJ, 680, 593

Tomsick, J. A., Krivonos, R., Wang, Q., et al. 2016a, ApJ, 816, 38

Tomsick, J. A., Rahoui, F., Krivonos, R., et al. 2016b, MNRAS, 460, 513

Ursini, F., Bassani, L., Malizia, A., et al. 2018, ATel, 11890, 1

Verner, D. A., Ferland, G. J., Korista, K. T., & Yakovlev, D. G. 1996, ApJ, 465, 487

Walter, R., Zurita Heras, J., Bassani, L., et al. 2006, A&A, 453, 133

Wilms, J., Allen, A., & McCray, R. 2000, ApJ, 542, 914

Winkler, C., Courvoisier, T. J.-L., Di Cocco, G., et al. 2003, A&A, 411, L1